Development 135, 53-63 (2008) doi:10.1242/dev.011437

Sisyphus, the *Drosophila* myosin XV homolog, traffics within filopodia transporting key sensory and adhesion cargos

Raymond Liu[1], Sarah Woolner[1,2,*], James E. Johndrow[1,*], David Metzger[1,*], Adriana Flores[1,*] and Susan M. Parkhurst[1,†]

Unconventional myosin proteins of the MyTH-FERM superclass are involved in intrafilopodial trafficking, are thought to be mediators of membrane-cytoskeleton interactions, and are linked to several forms of deafness in mammals. Here we show that the *Drosophila* myosin XV homolog, Sisyphus, is expressed at high levels in leading edge cells and their cellular protrusions during the morphogenetic process of dorsal closure. Sisyphus is required for the correct alignment of cells on opposing sides of the fusing epithelial sheets, as well as for adhesion of the cells during the final zippering/fusion phase. We have identified several putative Sisyphus cargos, including DE-cadherin (also known as Shotgun) and the microtubule-linked proteins Katanin-60, EB1, Milton and aPKC. These cargos bind to the Sisyphus FERM domain, and their binding is in some cases mutually exclusive. Our data suggest a mechanism for Sisyphus in which it maintains a balance between actin and microtubule cytoskeleton components, thereby contributing to cytoskeletal cross-talk necessary for regulating filopodial dynamics during dorsal closure.

KEY WORDS: Unconventional myosin, Myosin XV, Dorsal closure, Filopodia, Microtubules, Actin, Cytoskeleton, DE-cadherin (Shotgun), EB1, α-tubulin, *Drosophila*

INTRODUCTION

Epithelial movements underlie fundamental physiological processes including embryonic morphogenesis, wound healing and cancer metastasis (Ridley et al., 2003; Raich et al., 1999; Vasioukhin and Fuchs, 2001). During dorsal closure (DC), a morphogenetic event that occurs late in *Drosophila* embryogenesis, two lateral sheets of epithelial cells move towards one another over a dorsally exposed region of extraembryonic tissue and fuse together at the midline (Jacinto et al., 2002). During this process, the dorsal-most face of leading edge (LE) epithelial cells exhibit dynamic cellular protrusions, lamellipodia and filopodia, required initially for sensing their environment and finding their appropriate counterpart on the opposing epithelial sheet. Subsequently, the opposing protrusions adhere to one another, facilitating the formation of transient cell-cell contacts as the epithelial sheets zipper together, followed by permanent cell-adhesion structures. Filopodia contain a core of organized bundled actin filaments, oriented with their barbed (plus) ends towards the tip (Faix and Rottner, 2006). Filopodia continuously assemble and disassemble, with growth occurring via de novo actin nucleation and polymerization locally at their tips. Although the dynamic rearrangements of cells and filopodia during DC are mainly attributed to actin dynamics, a recent report has described a role for microtubules in epithelial zippering, the final step of DC (Faix and Rottner, 2006; Jankovics and Brunner, 2006).

The coordination of environmental sensing, cell-cell recognition and adhesion mediated by LE cell protrusions must require orchestrated movements of structural, adhesive and regulatory molecules within filopodia. Unconventional myosins have recently been implicated in the movement of such cellular molecules/machineries within filopodia (Mermall et al., 1998; Berg and Cheney, 2002). Unconventional myosins are actin-based motor proteins that can be subdivided into at least 18 distinct classes (I-XVIII) based on their motor and tail domain structural and functional characteristics (Oliver et al., 1999; Berg et al., 2001; Tzolovsky et al., 2002; Foth et al., 2006). One subset, the 'MyTH-FERM' unconventional myosins, includes classes VII, X, XII and XV that share structurally conserved features in their tails: MyTH4 (myosin tail homology 4) domains that bind to microtubules (Weber et al., 2004) and FERM (band 4.1, ezrin, radixin, moesin) domains that are involved in cargo binding (Sousa et al., 2005; Sheetz, 1999). The tail regions are thought to determine where the myosins are located and what cargos they transport (Oliver et al., 1999; Sheetz, 1999).

Mutations in MyTH-FERM unconventional myosins result in disorganized stereocilia leading to deafness and vestibular dysfunction in humans and mice: myosin VIIa is responsible for human Usher Syndrome type IB and the mouse *shaker 1* mutation, whereas myosin XV is linked to human non-syndromic deafness, DFNB3, and the mouse *shaker 2* mutation (Gibson et al., 1995; Weil et al., 1995; Liang et al., 1999; Libby and Steel, 2000). In *Dictyostelium*, Myosin VIIa (MVII) localizes to filopodial tips and is required for the formation of filopodia and cell attachment (Titus, 1999; Tuxworth et al., 2001). In mammalian cells, Myosin X (Myo10) moves bidirectionally within filopodia and accumulates at filopodial tips (Berg and Cheney, 2002; Bohil et al., 2006). Ectopic expression of Myo10 is sufficient to direct assembly of filopodia in cells lacking them. The Myo10 FERM domain has been shown to bind β-integrin and transport it to filopodial tips where it is needed for proper filopodial extension and substratum adherence (Zhang et al., 2004).

Drosophila has three MyTH-FERM myosin homologs: myosin VIIa, VIIb and XV (Tzolovsky et al., 2002). Functional data has only been reported for *crinkled* (myosin VIIa), mutants of which are semi-lethal with escaper adults exhibiting defects in actin-rich structures such as bristles and hairs (Kiehart et al., 2004), and deafness due to disruption of scolopidia auditory organ integrity required for transducing auditory signals (Todi et al., 2005).

[1]Division of Basic Sciences, Fred Hutchinson Cancer Research Center, Seattle, WA 98109, USA. [2]MRC-LMCB, University College London, London WC1E 6BT, UK.

*These authors contributed equally to this work
†Author for correspondence (e-mail: susanp@fhcrc.org)

Accepted 28 September 2007

In this study, we show that the *Drosophila* myosin XV homolog, which we named Sisyphus (Syph), is required for proper DC where it traffics sensory, cytoskeletal, and adhesion cargos within LE cells and their filopodial protrusions.

MATERIALS AND METHODS

Fly strains and genetics

Flies were cultured and crossed on yeast-cornmeal-molasses-malt and maintained at 25°C. Alleles used in this study were: P{en2.4-GAL4}e16E (Bloomington), P{UAS-GFP::lacZ.nls} (Bloomington), P{UASp-GFPS65C-alphaTub84B} (Bloomington), UAS-EB1-EYFP (D. Brunner, EMBL, Heidelberg, Germany), P{UAS-actin5C-GFP} (H. Oda, JT Biohistory Research Hall, Takatsuki, Japan), and P{UAS-shg.DEFL}6 (Kyoto).

We attempted to generate imprecise excisions using three different viable P-element lines inserted in or near the Syph locus (EY00595, EP1321 and NP-4100). We used a combination Southern blot and PCR analyses of potential excision lines to determine the molecular nature of the excision. Although we were able to generate many precise excisions, no imprecise excisions affecting Syph were obtained after screening >500 excision lines.

Sisyphus-GFP and Sisyphus-RFP were created by fusing either GFP or RFP ['Cherry' (Shaner et al., 2004)] C-terminal to the Syph ORF. The resulting Sisyphus-GFP or Sisyphus-RFP fusion constructs were cloned into pUASp as *Kpn*I-*Xba*I fragments and used to make germline transformants as described previously (Spradling, 1986). RFP-actin was made by fusing mRFP N-terminal to the ATG of the actin5C ORF and cloned into pUASp as a *Kpn*I-*Bam*HI fragment (P. Martin and S.M.P., unpublished). All transformant lines used in this study were mapped to a single chromosome and shown to have non-lethal insertions.

Nomenclature

The 'MyTH-FERM' subset of unconventional myosins, includes classes VII, X, XII and XV. *Drosophila* has three recognized MyTH-FERM unconventional myosins: a myosin VIIa homolog, Crinkled (CG7595); a myosin VIIb homolog, Myo28B1 (CG6976); and a myosin XV homolog, Myo10A (CG2174) (Tzolovsky et al., 2002). *Drosophila* does not have a class X homolog. We refer to the fly myosin XV homolog as Sisyphus, rather than its FlyBase name of Myo10A, to avoid confusion between the '10A' in this name (which refers to its cytological location on fly chromosomes) and class X unconventional myosins (of which it is not a member).

Antibody production and characterization

Polyclonal mouse antiserum against Syph was generated by immunizing BALB/c BYJ Rb(8.12) 5BNR/J mice (Jackson Labs) with a mixture of GST fusions to Syph amino acids 1608-1650, 2083-2115 or 2565-2602. These regions of Syph contain no homology to any other *Drosophila* gene. Antibody specificity was tested via western blot using in vitro translated full-length and tail fragments of Syph (see Fig. S1A in the supplementary material). This antibody also recognizes a doublet in extracts from DC staged wild-type *Drosophila* embryos (see Fig. 3B). Using this antibody (1:100 dilution), we find that Syph is maternally contributed and ubiquitously distributed in embryos (see Fig. S1C in the supplementary material and data not shown), and localizes to condensed chromosomes on the mitotic spindle (see Fig. S1D in the supplementary material).

Cell culture

Drosophila cell lines used in this study, S2R+, BG2 (ML-DmBG2) and EB1-GFP (S2-Mt-EB1-GFP) were obtained from the *Drosophila* Genomics Resource Center (DGRC; see https://dgrc.cgb.indiana.edu/cells/store/catalog.html for cell line description and references). S2R+ and EB1-GFP cells were grown at 25°C in Schneider's medium (Invitrogen) supplemented with 10% heat-inactivated FBS, 25 mM glutamine, penicillin and streptomycin. BG2 cells were grown at 25°C in Shields and Sang M3 medium (Sigma) with 25% bactopeptone (Difco), 10% yeast extract (BD), and supplemented as above.

RNA interference (RNAi)

Syph double-stranded RNA (dsRNA) was generated and either injected into embryos or placed on cells as previously described (Magie et al., 2002; Magie and Parkhurst, 2005). The regions of Syph used to generate dsRNA#1 (2480-2597aa) or dsRNA#2 (2391-2559aa) do not contain homology to other *Drosophila* genes as assayed by BLAST. Non-relevant RNAi constructs (GFP, α-catenin, p120catenin, or Rho1) do not produce the same phenotypes as Syph dsRNA when injected into embryos or put on cells (Magie et al., 2002; Magie and Parkhurst, 2005) (data not shown).

Immunofluorescence

Immunofluorescence of embryos and cells was performed as described previously (Magie and Parkhurst, 2005; Rosales-Nieves et al., 2006). The following antibodies were used in this study: α-DE-cadherin (1:10, a gift from H. Oda; also known as Shotgun – FlyBase), α-Groucho (1:400, a gift from C. Delidakis), and α-tubulin (1:500-1000, Harlan Sera-lab). Alexa Fluor 568- and Alexa Fluor 633-labeled phalloidin (Invitrogen) was used at 1-3 Units/assay and SlowFade Gold with DAPI (Invitrogen/Molecular Probes) was used to stain nuclei.

Confocal microscopy

Confocal microscopy was performed with a Zeiss LSM-510M with excitation at 488 nm, 543 nm, 633 nm or 780 nm (two-photon), and emission collection with BP-500-550, BP-565-615, BP-650-710 filters or BP-435-485 filters, respectively. An α-Plan-Fluor 100×/1.45 oil immersion, a Plan-Neofluor 40×/1.3 oil immersion, or a Plan-Apochromat 20×/0.75 dry objective was used for imaging. Post-acquisition images were processed with a 3×3 median filter in ImageJ, and assembled with Adobe Photoshop and Canvas software.

For live imaging, embryos were dechorionated and placed in halocarbon 700 oil on Greiner Lumox culture dishes made with hydrophilic gas permeable membranes (Sigma). For each movie, the figure panels corresponding to the movie, magnification, time interval between frames, and frame rate, are as follows. Movie 1: Fig. 2F-F‴, 160×, 3-4 minutes/frame, 3 frames/second; Movie 2: Fig. 2G-J, 240×, 4 seconds/frame, 7 frames/second; Movie 3, Fig. 4K-M, 160×, 2 seconds/frame, 25 frames/second; Movie 4, Fig. 6A-C, 240×, 2 seconds/frame, 25 frames/second.

Plasmids and constructs

This study used the following constructs: Syph-FL (1-2602aa from CG2174; accession no. AAF47983), Syph-tail (1295-2602aa), Syph-t1 (1295-2082aa), Syph-t2 (2083-2273aa), Syph-t3 (2274-2602aa), Syph-L1 (2259-2373aa), Syph-L2 (2374-2476aa), Syph-L3 (2477-2573aa), Syph-E (2574-2602aa), Syph-L1a (2259-2331aa), Syph-L1b (2332-2373aa), Syph-L1a1 (2259-2284aa), Syph-L1a2 (2285-2305aa), Syph-L1a3 (2306-2330aa), Syph-L3a (2477-2530aa), Syph-L3b (2531-2573aa), cad^{ICD} (1346-1507aa from CG3722; accession no. AAF46659), cad-A (1346-1390aa), cad-B (1391-1438aa), cad-C (1439-1466aa), cad-D (1467-1507aa), Katanin-60 (1-572aa from CG10229; accession no. AAF52059), aPKC (1-606aa from CG10261; accession no. AAF58177), Milton (1-1122aa from CG13777; accession no.AAN10622), and EB1 (1-291aa from CG3265; accession no.AAM70826). Syph-L1 substitution point mutations (LGVE*, SEAEQ*, QEF*, SLYC*, IVQG* and DAFT*) were made within the Syph-L1 fragment (2259-2373aa) using primers that substitute alanines for the amino acids indicated. Syph-L3 substitution point mutations (HWS*, STR* and DMK*) were made within the Syph-L3 fragment (2477-2573aa) using primers that substitute alanines for the amino acids indicated. These constructs were cloned into pCite (Novagen), pGEX (GE) or pRSET (Stratagene) vectors using standard PCR cloning techniques.

Protein expression, GST-pulldown assays and immunoprecipitations

Protein expression, GST pulldown assays and immunoprecipitations were performed as previously described (Magie and Parkhurst, 2005; Rosales-Nieves et al., 2006).

Yeast two-hybrid interactions and screening

Yeast two-hybrid interactions and screening were performed with a LexA fusion to the Syph C-terminal tail (1295-2602aa) using a *Drosophila* early embryo library as previously described (Poortinga et al., 1998). Putative Syph interactors were confirmed in a yeast mating assay as previously described (Poortinga et al., 1998), with a subset of the interactors also confirmed using GST pulldown assays (see Fig. 3, Table 1, and Fig. S2A in the supplementary material).

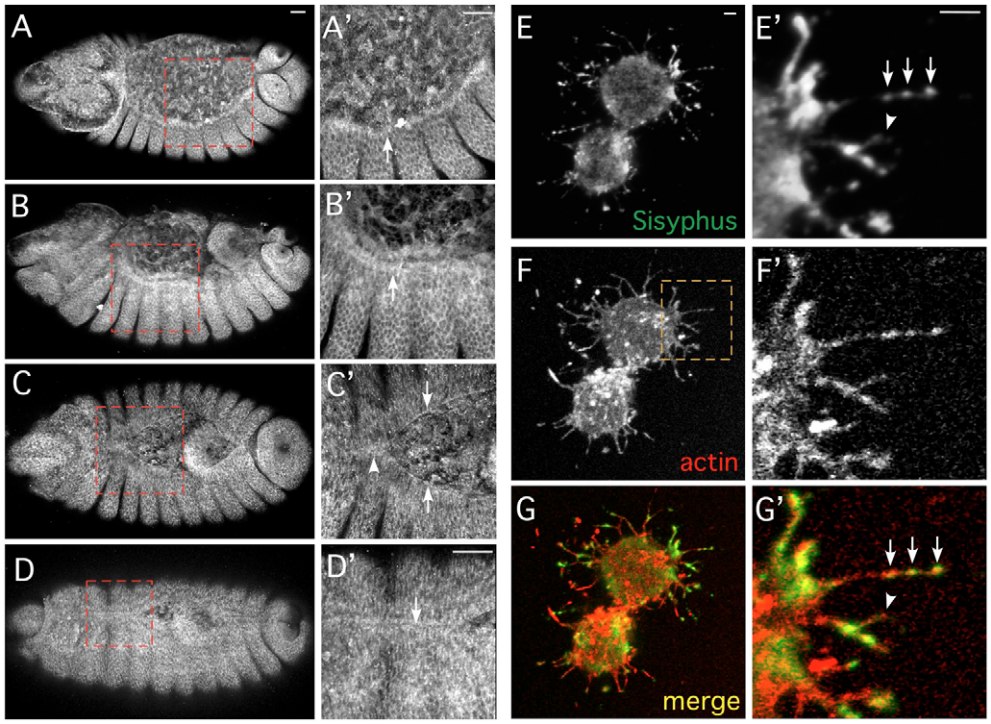

Fig. 1. Distribution of Syph in *Drosophila* embryos and S2R+ cells. (**A-D**) Dorsal view of successively older wild-type stage 14 *Drosophila* embryos stained with an anti-Syph antibody. Boxed regions are shown at higher magnification in **A′-D′**. Syph is predominantly cytoplasmic at this stage. Note Syph accumulation in the leading edge (LE) cells (arrows in A′,B′) before the onset of dorsal closure (DC). This accumulation resolves to the dorsal-most edge of LE cells (arrows in C′) and seam edge (arrowhead) during DC, and then subsides once closure is complete (arrow in D′). (**E-G**) S2R+ cells stained with an anti-Syph antibody (E,E′; green in G,G′) and phalloidin to visualize actin (F,F′; red in G,G′). The boxed region in F is shown at higher magnification in **E′-G′**. Syph is found along filopodial extensions and at a subset of their tips (arrows in G′), but not all tips (arrowhead in E′ and G′). Scale bars: 20 μm in A-D′; 2 μm in E-G′.

RESULTS

Syph protein accumulates in LE cells and filopodia

As MyTH-FERM unconventional myosins are good candidates for playing a role in embryonic morphogenesis, we examined the distribution of Syph throughout embryonic development using a mouse polyclonal antibody generated against the C-terminal tail of Syph (see Materials and methods; see Fig. S1 in the supplementary material). Sisyphus is maternally contributed and ubiquitously distributed (see Fig. S1 in the supplementary material). At the cellular stages, Syph protein is present in the nucleus and throughout the cytoplasm of all embryonic cells, as well as the extraembryonic amnioserosa cells (Fig. 1A-D). We focused on the stages surrounding and immediately preceding DC where we observed an accumulation of Syph protein in the LE cells (Fig. 1A′,B′). By the zippering stage of DC, this Syph accumulation resolves to the dorsal-most surface of the LE cells as the two epithelial edges meet (Fig. 1C′), and subsides once closure is complete (Fig. 1D′).

MyTH-FERM unconventional myosins have been shown to localize to the tips of filopodia (Tuxworth et al., 2001; Berg and Cheney, 2002). We examined Syph localization in *Drosophila* S2R+ and BG2 cells (see Materials and methods) and observed Syph localization in puncta along filopodia, as well as throughout the cell body (Fig. 1E-G; Fig. 4H,H′). Similar to other MyTH-FERM myosins, Syph localizes to the ends of filopodia, but unlike them, it does not accumulate preferentially at their tips (Fig. 1E′,G′).

Dynamic localization of Syph during dorsal closure

To further investigate the role of Syph in LE cells of the embryo in vivo, we generated *Drosophila* lines carrying GFP or RFP fusions to Syph under the control of the conditional UAS promoter. Driving expression of the fluorescent fusion proteins in epithelial stripes with an Engrailed (En)-Gal4 driver (Brand and Perrimon, 1993), we observed accumulation of Syph at the leading edge during DC (Fig. 2A-E′). As seen with antibody staining, this accumulation intensifies just prior to and during epithelial edge matching (Fig. 2A′,F-F‴), but subsides after the edges have met and fused (Fig. 2E′). At higher magnifications we observed punctate accumulations of Syph at the dorsal-most edge of LE cells and in filopodia extending from their dorsal-most edge (Fig. 2F-L″). As filopodia from opposing epithelial edges meet and adhere, the punctate accumulation appears to migrate into the newly formed junction (Fig. 2F-F‴ and see Movie 1 in the supplementary material).

To examine the dynamics of Syph localization within filopodia, we captured time-lapse confocal images of LE filopodia (Fig. 2G-J′ and see Movie 2 in the supplementary material). The filopodia themselves were very dynamic, growing and moving between frames. Within filopodia, we observed punctate dots and bands of Syph that move along the length of the filopodia. Although Syph can be observed at the tips of filopodia, this accumulation is not permanent; rather Syph appears to be in constant motion along the filopodia.

Identification of Syph cargo proteins

Since Syph protein localization suggests that it traffics proteins within LE cells and their filopodia, we performed a yeast two-hybrid screen with the C-terminal cargo-binding (tail) region of Syph to identify its cargos (see Materials and methods). We identified 25 potential cargos, including DE-cadherin and several microtubule (MT)-regulating proteins (Table 1). DE-cadherin was of particular interest because mutations in human cadherin-23 and protocadherin-15 are also linked to Usher syndrome (Reiners et al., 2006). The MT-associated cargos, including α-tubulin, atypical protein kinase C (aPKC), the MT severing protein Katanin-60, the MT transport protein Milton (Milt), and the MT plus-end (+TIP) binding protein EB1, were also of interest because MTs have been recently been shown to play an essential role in DC (Jankovics and Brunner, 2006) and in filopodial dynamics (Rodriguez et al., 2003; Schober et al., 2007).

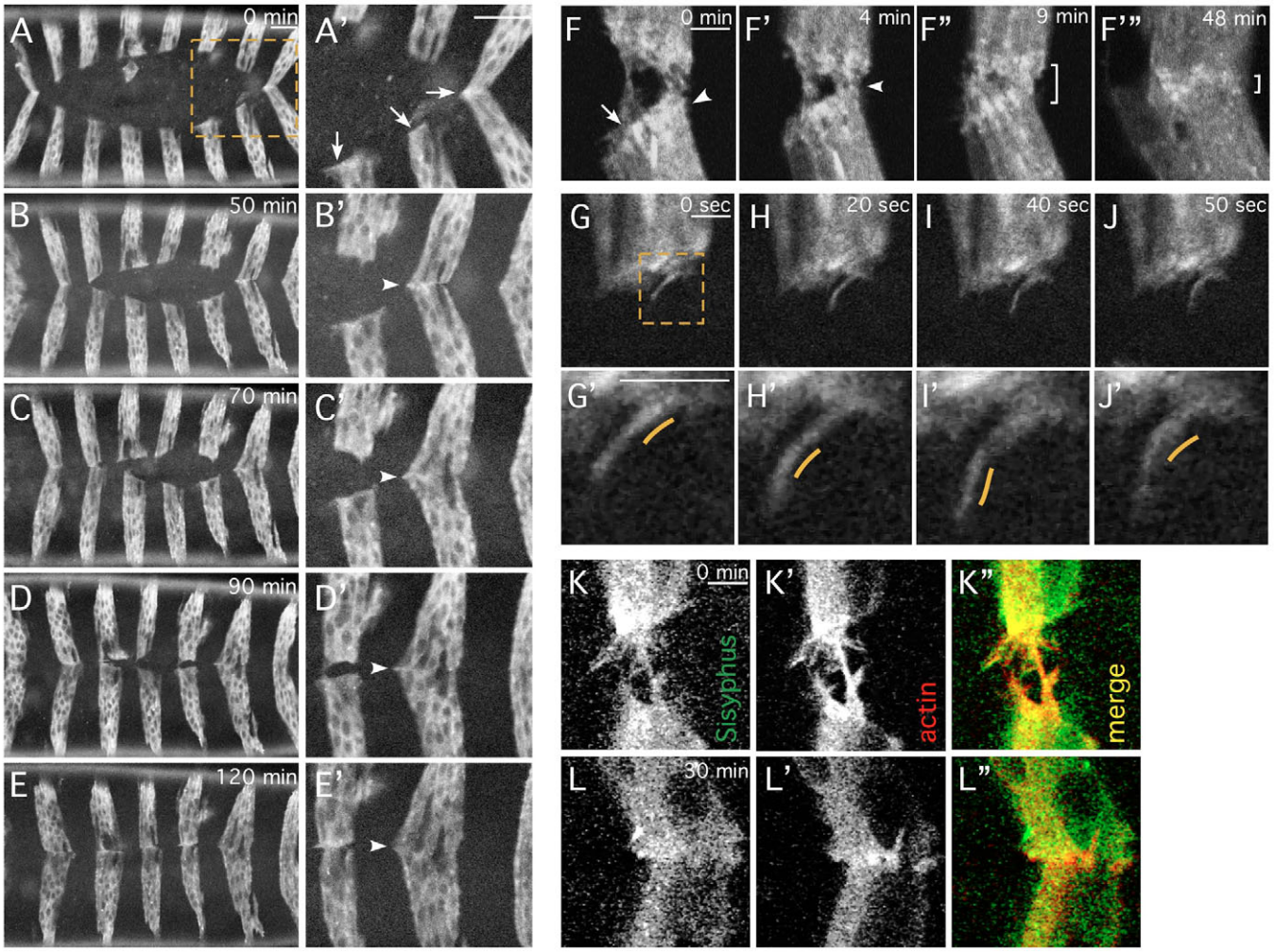

Fig. 2. Syph is dynamically expressed in LE cells and filopodia during DC. (**A-E**) Dorsal view of an embryo expressing Syph-RFP in an En (striped) pattern during DC. Boxed region in A and equivalent regions of B-E are shown at higher magnification in **A′-E′**. Note that Syph accumulates in LE cells as the epithelial sheets meet (arrows in A′), and decreases after midline fusion. (**F-F‴**) Syph accumulates in puncta at the apex of LE cells expressing GFP-Syph (arrow in F). These puncta accumulate in filopodia as the epithelial sheets meet (arrowhead in F,F′) and disperse after cell fusion (brackets in F″-F‴). See Movie 1 in the supplementary material. (**G-J**) Syph localization in filopodia. Boxed region in G and equivalent regions of H-J are shown at higher magnification in G′-J′. Levels of Syph are dynamic within a growing filopodia: yellow lines in **G′-J′** follow the movement of a Syph puncta within a single filopodia. See Movie 2 in the supplementary material. (**K-L″**) Filopodia in LE cells in an embryo expressing both Syph-GFP (K,L; green in K″,L″) and mRFP-actin (K′,L′; red in K″,L″) in an En pattern. As epithelial sheets approach each other, both Syph and actin accumulate in the LE cells and in their filopodia (K-K″), before resolving to a thin band of expression at the dorsal-most edge after fusion (L-L″). Scale bars: 20 μm in A-E′; 5 μm in F-L″.

To confirm that the proteins we identified are bona fide Syph cargos, we performed GST pulldown assays with GST fusions to a subset of these proteins (Fig. 3A; see Fig. S2A,B in the supplementary material). Consistent with their predicted roles as Syph cargos, Katanin-60, aPKC, Milt, EB1 and the intracellular domain of DE-cadherin (cad^{ICD}) all bind the C-terminal tail region of Syph (Fig. 3A). To verify that these interactions occur in vivo, we co-immunoprecipitated Syph-containing complexes from *Drosophila* embryo lysates. Given the disease relevance of E-cadherin and the availability of reagents, we focused on the interaction between Syph and cad^{ICD}. Western blot analysis of these Syph-immunoprecipitated complexes reveals the presence of DE-cadherin (Fig. 3B), confirming the in vivo relevance of this interaction.

We mapped the binding sites for cad^{ICD} on Syph using smaller Syph protein constructs in GST pulldown assays (Fig. 3C-E). The cad^{ICD} binds to the t3 fragment of Syph (Fig. 3C,D), which contains the conserved FERM domain. Upon further mapping, we were surprised to find that the cad^{ICD} binds to two distinct regions of the FERM domain: one within the Lobe 1 (L1) region (L1a3; aa2259-2330) and one within the Lobe 3 (L3) region (L3b; aa2531-2573) (Fig. 3C-E). This finding, however, is consistent with the solved crystal structure of the Merlin FERM domain (Kang et al., 2002), which shows that the regions corresponding to L1 and L3 are structurally adjacent (Fig. 3J-J″), forming a surface fit for binding cargo.

In parallel, we mapped the binding of Katanin-60, aPKC and Milt to the same two distinct regions of the Syph FERM domain (Fig. 3F-G; data not shown). We attempted to generate mutants that were defective in binding of specific cargos using a series of targeted three to four amino acid substitution mutations within the context of Syph protein fragments encompassing either the L1 or L3 regions (Fig. 3C; data not shown). Point mutations that abolish cad^{ICD} binding (IVQG*, DAFT*, STR* and DMK*) also abolish the binding of Katanin-60 and Milt, but not that of aPKC (Fig.

Table 1. Sisyphus (myosin XV) interactors and potential cargoes

Gene	Designation	Cytological location	Physical interaction*	Biological process
DE-cadherin/shotgun	CG3722	57B15-16	Yes	Transmembrane adhesion molecule; adherens junction component
α-Tubulin	CG2512	84D	Yes	Microtubule subunit
katanin 60	CG10229	82F6	Yes	Microtubule binding/severing
Eb1	CG3265	42C8	Yes	Microtubule tip binding (+TIP)
milton	CG13777	27D5-7	Yes	Affects kinesin- and dynein-dependent transport of mitochondria
atypical protein kinase C (*aPKC*)	CG10261	51D5-6	Yes	Cell polarity/asymmetrical protein localization; zonula adherens assembly
karyopherin α3	CG9423	85D25	Yes	Protein import into nucleus; regulates heat-shock response
Heat shock protein 26	CG4183	67B2	Yes	Small developmentally regulated heat-shock protein
smaug	CG5263	66F1	Yes	RNA/protein binding; RNA localization; translational repression
Nedd4	CG7555	74D2-3	Yes	Ubiquitin protein ligase; regulates endocytosis
cleavage and polyadenylation specificity factor (*cpsf*)	CG10110	51A4	Yes	mRNA binding
Suppressor of Cytokine Signaling at 16D (*Socs16D*)	CG8146	16D4	Yes	Suppressor of cytokine signaling; signal transduction
Brahma assisted protein 60kD (*Bap60*)	CG4304	11E1	NT	Brahma complex component; chromatin remodeling complex
tango	CG11987	85C2	No	HLH transcription factor
cropped	CG7664	35F1	Yes	Transcription factor
Ribosomal protein L23 (RpL23)	CG3361	59B3	NT	Ribosomal protein (RpL17A)
Ribosomal protein L34a (RpL34a)	CG6090	96F10	NT	Ribosomal protein
–	CG17033	72B2-C1	Yes	Unknown; RING finger
–	CG1078	82B3-4	Yes	Unknown
–	CG6834	86E15-16	Yes	Unknown
–	CG2258	7D6	Yes	Unknown
–	CG18135	75F2	Yes	Unknown
–	CG32810	2B1	NT	Unknown; BTB/POZ domain
–	CG2765	60E10-11	NT	Unknown
–	CG5613	16A5	NT	Unknown

Protein interactors from yeast two-hybrid screen with Sisyphus C-terminal tail fragment.
NT, not tested.
*Yes, physical interaction confirmed in GST pull-down assays (see Fig. 3 and Fig. S2 in the supplementary material).

3F,G). Thus, our results suggest that although Syph could transport some of its cargos simultaneously, transport of others is probably mutually exclusive.

Conversely, we mapped the region of cad^{ICD} that binds Syph. We divided the cad^{ICD} into four pieces (cadA-D) (Fig. 3H; see Fig. S2C in the supplementary material), and find that Syph binds the most C-terminal 40aa piece, cad-D (aa1467-1507) (Fig. 3H,I). This interaction domain has not previously been assigned a function, but is conserved in human cadherins (see Fig. S2D in the supplementary material).

Syph is required for proper dorsal closure

To determine whether Syph protein accumulation in LE cells and filopodia has a functional role, we examined DC in *syph*-deficient embryos. Since specific *syph* mutations have not yet been reported and we were unable to generate one using imprecise P-element excision (see Materials and methods), we used dsRNA interference (RNAi) to specifically reduce Syph protein levels and disrupt Syph function (see Materials and methods; see Fig. S3 in the supplementary material). We injected two different Syph dsRNAs, an unrelated dsRNA (i.e. GFP), or buffer alone into embryos expressing a UAS-GFP-actin fusion construct (Verkhusha et al., 1999) under the control of the En-Gal4 driver to express the GFP-actin fusion protein in alternating epidermal stripes, and followed their development during DC. In buffer-injected embryos, DC proceeded normally and was complete in 2.5-3 hours. Cells within a given segment matched with their counterpart on the opposing side during epithelial zippering, as indicated by the correct alignment of En pattern stripes in 96% (n=248) of embryos (Fig. 4A-A‴). Injection of an unrelated dsRNA (GFP) also resulted in correct alignment of En pattern stripes in 98% (n=64) of embryos (see Fig. S3B-C in the supplementary material). In *syph* dsRNA-injected embryos, although DC was complete within 3 hours, we observed mismatching of segments in ~38% of embryos (39%, n=229 for dsRNA #1; 37%, n=99 for dsRNA #2). As the two Syph dsRNAs produce identical phenotypes, we show only dsRNA #1 from this point. In these mismatching cases, one stripe (four cells), or even a single LE cell, would broaden and contact several cells on the opposing epithelium (Fig. 4B-C‴,F,G). Thus, Syph is required for proper environmental sensing and cell-cell recognition during DC.

Syph is required for proper localization of cadherin to the leading edge

Since Syph and cadherin show direct molecular association, we examined their subcellular localization in embryos and cells. Live imaging of DC-staged embryos expressing cadherin-GFP and Syph-RFP showed that both proteins are present in LE cell protrusions, albeit at lower levels than actin-GFP (data not shown). However, as the embryo LE cell filopodia were too dynamic for capture of live dual-fluor confocal images, we co-stained *Drosophila* BG2 and S2R+ cells, both of which exhibit numerous filopodia. Consistent with their direct molecular interaction in vitro, Syph and cadherin co-localize in puncta along the filopodia (Fig. 4H-J′; data not shown).

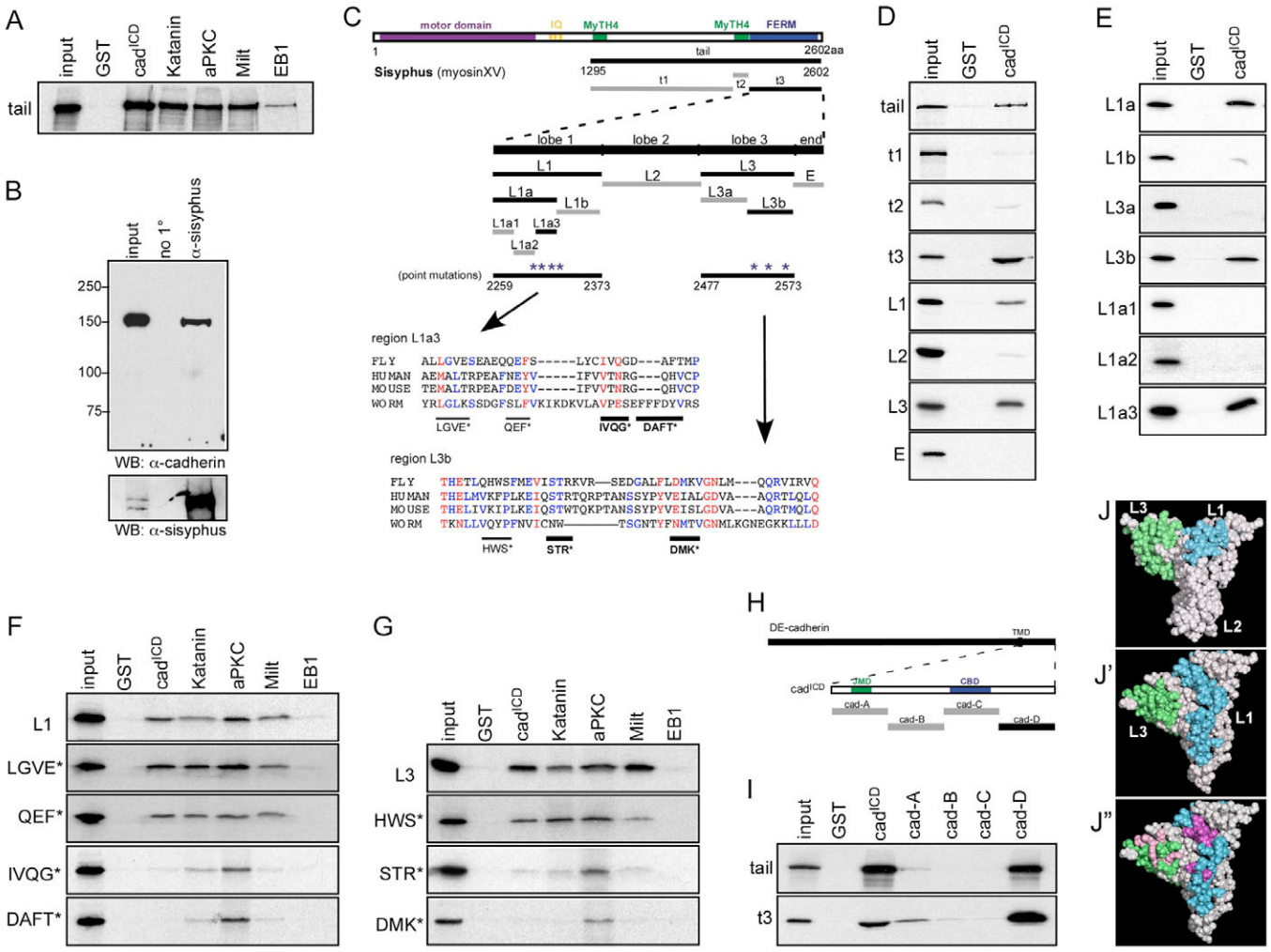

Fig. 3. Syph interacts with DE-cadherin and several MT-associated proteins through its FERM domain. (**A**) ^{35}S-labelled in vitro translated (IVT)-Syph C-terminal tail (input) binds to GST-cad^{ICD}, -Katanin, -aPKC, -Milt and -EB1. (**B**) DE-cadherin was immunoprecipitated from embryo lysate with an anti-Syph antibody, but not when primary antibody was omitted. (**C**) Diagram of the Syph protein fragments and substitution point mutations used to map protein-protein interactions. (**D**,**E**) GST-cad^{ICD} binds ^{35}S-labelled IVT-Syph tail, -Syph t3, and the -L1 and -L3 regions of the Syph FERM domain. GST-cad^{ICD} binding maps to the L1a3 fragment within the L1 region and the L3b fragment within the L3 region. (**F**,**G**) Substitution point mutations in the L1 or L3 regions do not selectively inhibit cad^{ICD} binding to Syph. GST-cad^{ICD} and -Milt bind to ^{35}S-labelled IVT-L1, -L3, -LGVE*, -QEF* and -HWS*, but show significantly reduced binding to IVT-IVQG*, -DAFT*, -STR* and -DMK*. GST-Katanin binds to IVT-L1, -L3, and all of the mutant fragments except IVT-DMK*. GST-aPKC binds to IVT-L1, -L3, and all the mutant proteins tested. EB1 binding does not map to the L1 or L3 regions and serves as a negative control. (**H**) Diagram of DE-cadherin protein and the protein fragments used to map its interaction with Syph. JMD: juxtamembrane domain, CBD: catenin binding domain; TMD: transmembrane domain. (**I**) ^{35}S-labelled Syph-tail and -t3 proteins bind to GST-cad^{ICD} and -cad-D. (**J-J″**) Computer model of the Merlin FERM domain crystal structure. The regions corresponding to L1 and L3 in Syph are shown in green and blue, respectively, and lie on the same surface of the protein as shown in side (J) and topdown (J′) views. (J″) The position of the point mutations in L1 and L3 that disrupt Syph binding to cad^{ICD} are shown in purple and pink, respectively.

To test whether the *syph*-deficient embryos exhibit mismatching because of cadherin mislocalization, we injected Syph dsRNA or buffer alone into embryos expressing a GFP-DE-cadherin (Oda and Tsukita, 1999) fusion protein. In buffer-injected embryos, 98% (n=50) developed normally (no-mismatching). We observed localized accumulation of GFP-cadherin at the dorsal-most surface and in filopodia of the LE cells (Fig. 4D-D‴,K; see Movie 3 in the supplementary material). In *syph* dsRNA-injected embryos, we observed a mismatching phenotype similar to that observed with the GFP-actin-expressing embryos, as well as abnormal constriction of the LE cells in opposing segments as a result of cells reaching laterally and matching with other adjacent cells (68% exhibit mutant phenotypes; n=117; Fig. 4E-E⁗). Surprisingly, these embryos progressed more slowly and failed to close during the time they were observed (about 9 hours), which was 4-5 hours longer than wild-type or the buffer-injected control embryos.

The localized accumulation of GFP-cadherin at the dorsal-most surface of LE cells observed in buffer-injected embryos (Fig. 4K; see Movie 3 in the supplementary material) was reduced in *syph*-deficient embryos that exhibited mismatching, and filopodia were mostly absent in their LE cells (Fig. 4M; see Movie 3 in the supplementary material). *Syph*-deficient embryos that showed proper epithelial matching exhibited an intermediate phenotype: some localized accumulation of GFP-cadherin at the dorsal-most edge of LE cells could be detected, and these embryos displayed predominantly lamellipodia-like extensions rather than filopodia at

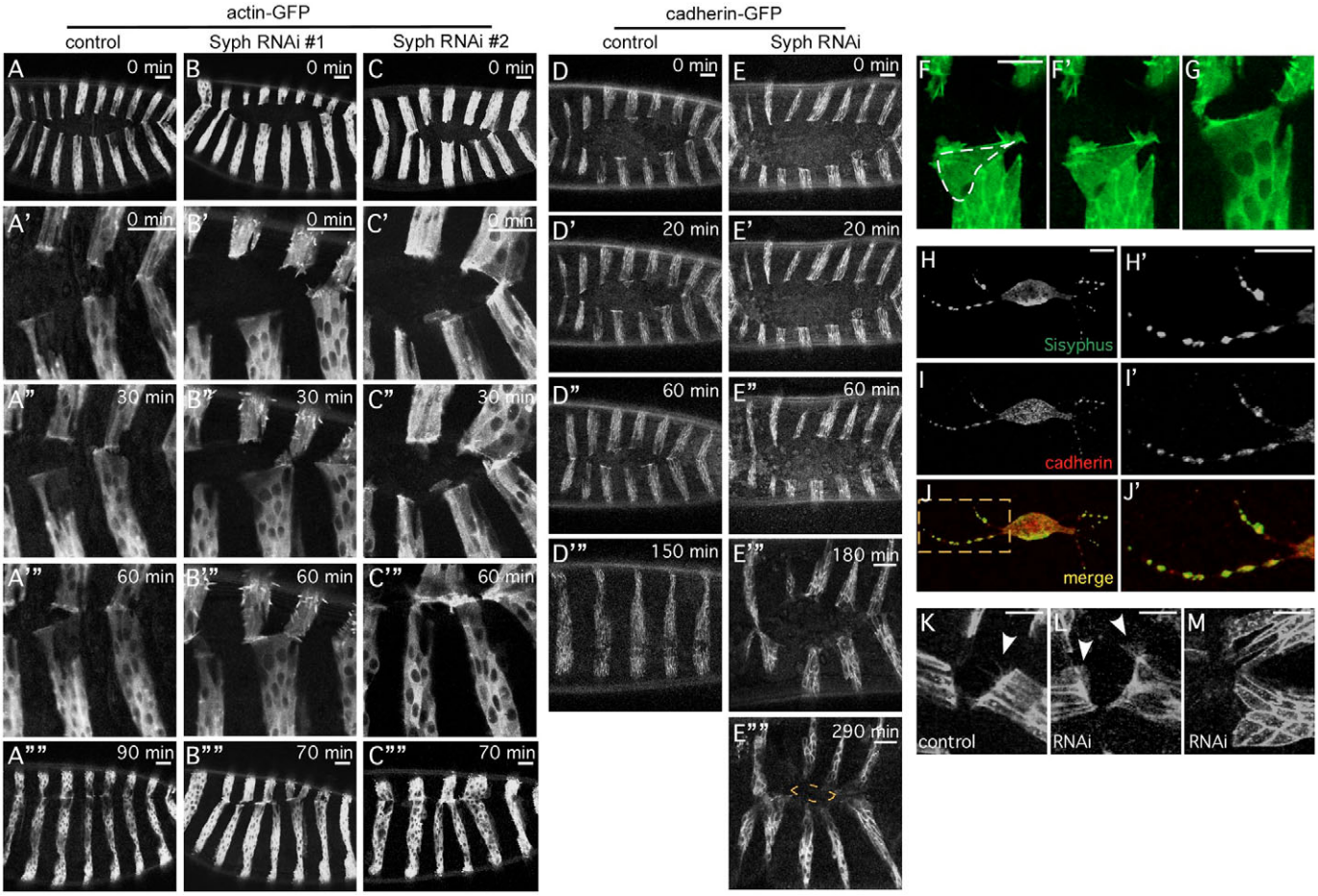

Fig. 4. *syph*-deficient embryos exhibit delayed and mis-matched epithelial alignment during DC. (**A-E''''**) Confocal micrographs showing dorsal view of an embryo expressing actin-GFP (A-C'''') or DE-cadherin-GFP (D-E'''') under the control of the En-Gal4 driver (striped pattern) that were injected with buffer alone (A-A'''',D-D''), with Syph dsRNA#1 (B-B'''',E-E''), or with Syph dsRNA#2 (C-C'''') undergoing DC. Syph RNAi-injected embryos expressing the actin-GFP reporter complete DC but show mismatching of stripes, whereas those expressing the cadherin-GFP reporter display mismatched, puckered stripes and delayed or incomplete hole closure (see oval in E''''). Note: the intense actin-GFP labeled filopodia on the upper side of the embryo in B'-B''' are observed as a result of the orientation of the embryo, not as a result of the Syph RNAi. (**F-G**) Confocal micrograph of a single optical plane from two time points (F, F', and G, respectively) of Syph RNAi-injected embryo expressing En-Gal4 driven actin-GFP showing a single cell from one epithelial sheet (dashed line) contacting across eight to ten cells from the opposite epithelial sheet. (**H-J'**) BG2 cell co-stained for Syph (H) and DE-cadherin (I) show co-localization of the two proteins in filopodia (J). (H'-J') Higher magnification view of the area boxed in J for H-J, respectively. (**K-M**) High magnification dorsal view of embryos expressing DE-cadherin-GFP under the control of the En-Gal4 driver (striped pattern) that were injected with buffer alone (K) or with Syph dsRNA#1 (L,M) undergoing DC. Note accumulation of GFP-cadherin at the dorsalmost side of the LE cells and the long filopodial extensions in control (arrowhead, K) embryos. Syph-deficient embryos that exhibit epithelial mismatching do not accumulate GFP-cadherin on the dorsal-most side of their LE cells or appreciable filopodia (M), whereas Syph-deficient embryos that can still match their epithelial sheets display an intermediate phenotype with some dorsal edge GFP-cadherin accumulation and lamellipodia-like projections from their LE cells (arrowheads, L). See Movie 3 in the supplementary material. Scale bars: 20 μm in A-E''''; 10 μm in F-M.

their leading edges (Fig. 4L; see Movie 3 in the supplementary material). Syph is thus important for correct localization of cadherin to the leading edge during DC.

Overexpression of actin partially rescues *syph*-deficient mutant phenotypes

Although injection of Syph RNAi into GFP-actin- or GFP-cadherin-expressing embryos results in mismatching, the additional phenotypes we observe in the GFP-cadherin-expressing embryos (slowing of closure times and failure to close the hole) suggested to us that overexpression of the fluorescently tagged proteins (GFP-actin or GFP-cadherin) may be affecting Syph functions, thereby modulating cytoskeletal architecture/dynamics. We considered two possibilities: either GFP-actin overexpression is suppressing the slowing and failure to close phenotypes associated with the loss of Syph, or overexpressed cadherin is exacerbating it. To distinguish between these possibilities, we injected Syph dsRNA or buffer alone into embryos expressing a nuclear-tagged GFP protein that should not affect cytoskeletal architecture (or into wild-type embryos; see Fig. S3F-H in the supplementary material). In buffer-injected embryos, the opposing segments matched up correctly and closure was complete by 3 hours in 95% (n=135) of nuclear-GFP-expressing embryos (Fig. 5A-A''''). In embryos injected with Syph dsRNA (42%, n=132), closure was slowed and the midline seam puckered and failed to fully close (Fig. 5B-B''''). This phenotype resembles that observed with GFP-cadherin (Fig. 4D-D''''), and suggests that

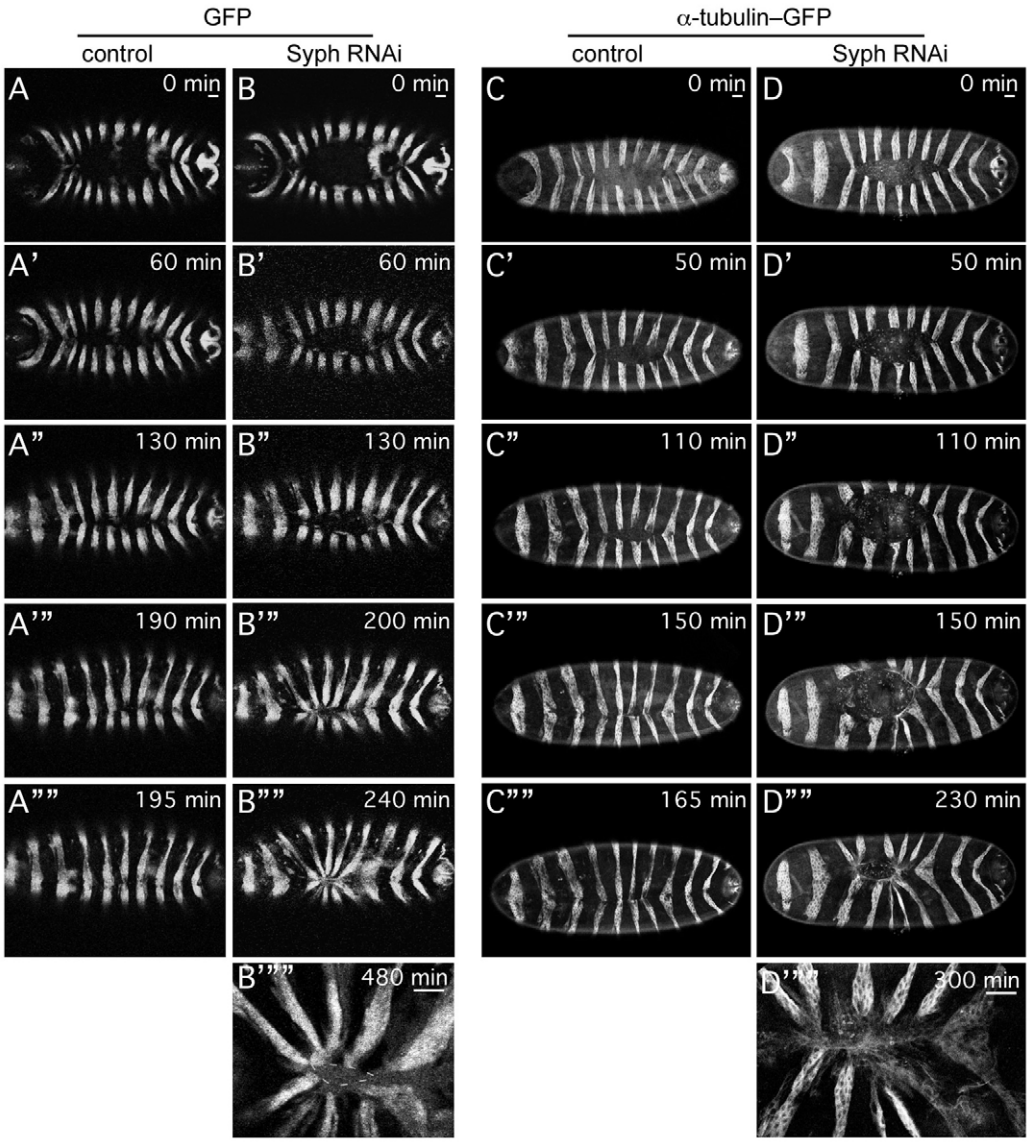

Fig. 5. *syph*-deficient embryos exhibit disrupted MT networks. (**A-D""'**) Confocal micrographs showing dorsal view of embryos expressing nuclear GFP (A-B"") or α-tubulin-GFP (C-D"") under the control of the En-Gal4 driver, which were injected with buffer alone (A-A"', C-C"") or with Syph dsRNA (B-B"", D-D"") undergoing DC (time elapsed intervals given in minutes). Syph RNAi-injected embryos exhibit misaligned stripes and delayed or incomplete dorsal hole closure. Scale bars: 20 μm.

actin overexpression partially rescues the 'delayed' and 'failure to close' phenotypes of *syph*-deficient embryos. The retardation of DC progression resembles that of embryos with disrupted MTs: ectopic expression of the spastin MT severing protein (triggering MT disassembly) resulted in delayed epithelial closure (~9 hours) (Jankovics and Brunner, 2006). Although this ectopic spastin expression did not affect filopodial environment sensing or cell-cell recognition during DC, it did disrupt the final step of zippering when adhesions are formed.

Since GFP-actin appears to partially rescue the 'delayed' and 'failure to close' phenotypes of Syph RNAi and because MT severing causes a similar delay in closure, we hypothesized that overexpression of MTs might also rescue the delay phenotype. Overexpression of MTs would require co-expression of both α- and β-tubulin; lack of a UAS-β-tubulin fly line permitted us to only inject into embryos overexpressing GFP-α-tubulin. In control buffer-injected embryos, the opposing segments matched up correctly and closed within 3 hours in 99% (n=83) of embryos (Fig. 5C-C""). In embryos injected with Syph dsRNA (69%, n=121) we observed an intermediate phenotype. DC progression was slowed (⩾5 hours) and advancing segment stripes puckered, similar to that observed with embryos expressing GFP-cadherin (Fig. 4D-D"") or GFP alone (Fig. 5B-B""). However, after about 5 hours, fusion of the stripes occurred and a midline seam was observed. We conclude that overexpression of GFP-α-tubulin does not rescue the abnormal phenotypes to the extent that overexpression of GFP-actin does. The apparent rescue of the closure phenotype, though, leaves open the intriguing possibility that overexpression of both α- and β-tubulin, and thus MTs, may result in stronger rescue.

Syph is required for filopodia dynamics and cargo localization

The above results suggest that Syph has important roles in: (1) the transport of essential cargo proteins required for proper segmental matching and zippering to the leading edge, and (2) the modulation of cytoskeletal architecture and dynamics. To further explore the first half of this hypothesis, we took advantage of a newly created line of EB1-EYFP-expressing flies (Jankovics and Brunner, 2006) to test the effect of Syph removal on the trafficking of EB1, a putative Syph cargo. In buffer-injected embryos, EB1-EYFP could be seen to move dynamically within the cells expressing it and within the numerous filopodial extensions at the dorsal-most edge

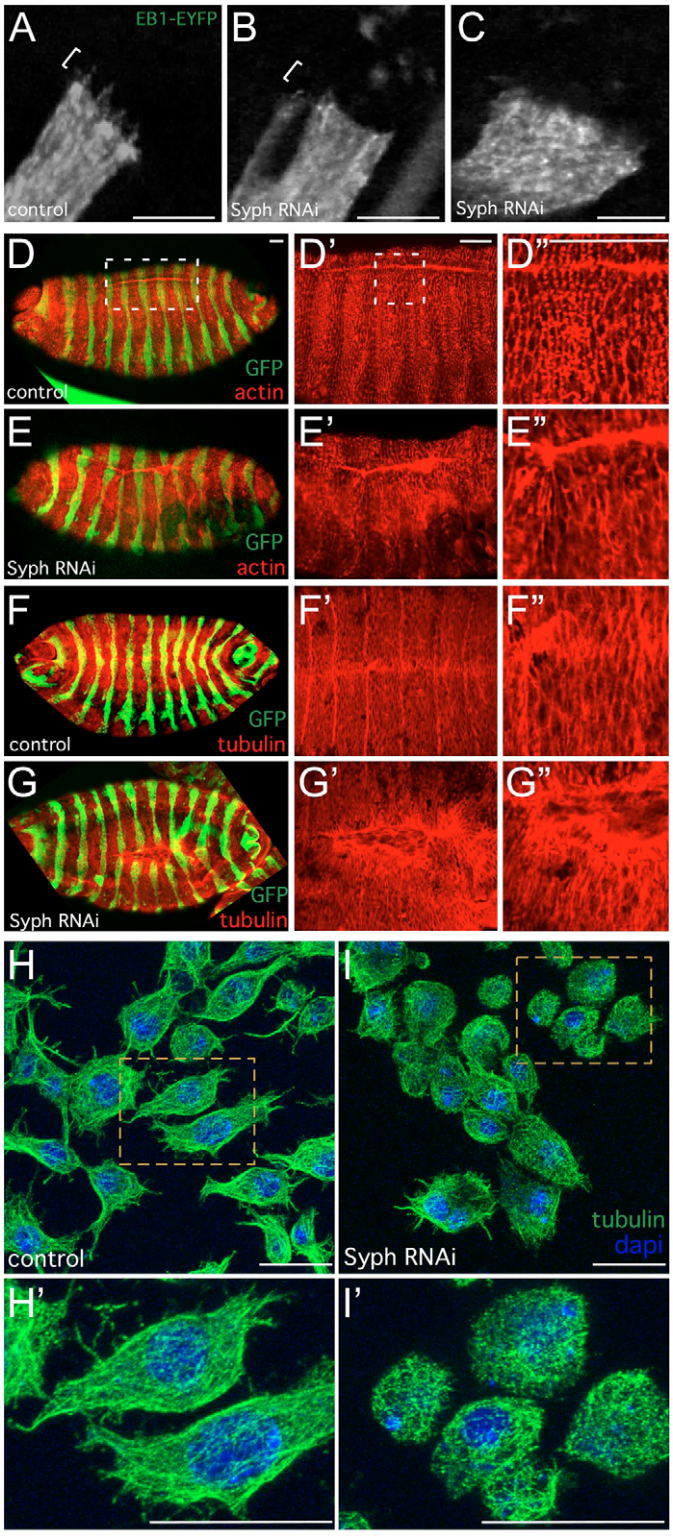

Fig. 6. Aberrant localization of Syph cargos in *syph*-deficient embryos. (**A-C**) High-magnification dorsal view of embryos expressing EB1-EYFP under the control of the En-Gal4 driver (striped pattern) that were injected with buffer alone (A) or with Syph dsRNA (B,C) undergoing DC. Note trafficking of EB1-EYFP LE cell filopodia (brackets) in control embryos (A) that is mostly absent from Syph-deficient embryos (bracket, B; C). Syph-deficient embryos exhibiting the strongest phenotypes also show disrupted EB1-EYFP trafficking within the LE and more ventrally located cells (C). See Movie 4 in the supplementary material. (**D-G″**) Actin expression (as visualized by phalloidin staining; D-E″) and α-tubulin expression (F-G″) in buffer-injected (D-D″; F-F″) and Syph dsRNA-treated (E-E″; G-G″) nuclear-GFP-expressing stage 15 embryos. (**H-I′**) α-tubulin expression in wild-type (H,H′) and Syph dsRNA-treated (I,I′) S2R+ cells. Note reduction of cellular extensions and disruption of MT lattice networks in the Syph RNAi-treated cells. Scale bars: 10 μm in A-C; 20 μm in D-I′.

of the LE cells (Fig. 6A). *Syph*-deficient embryos displayed slower movement of EB1-EYFP within the cells expressing it (9.0±2.4 μm/minute, compared with 11.4±2.9 μm/minute for wild-type, as determined by kymographic analysis; $P<0.0003$). In addition, *syph*-deficient embryos have fewer filopodia extensions with a concomitant increase in lamellipodia (Fig. 6B; see Movie 4 in the supplementary material). In the most severely disrupted *syph*-deficient embryos, trafficking of EB1-EYFP within LE cells is disrupted such that the predominantly apical-basal movement seen in control embryos becomes randomly oriented (7.1±2.0 μm/minute; Fig. 6C; see Movie 4 in the supplementary material). Since EB1 is a microtubule tip binding (+TIP) protein, this may also reflect a disruption of the cytoskeleton and suggests a role for Syph in regulating cytoskeletal architecture.

To examine how Syph may modulate cytoskeletal architecture, we examined actin and MT expression in *syph*-deficient embryos and cells. Consistent with the actin and tubulin GFP reporter constructs in live imaging, *syph*-deficient embryos show disruptions to both actin and MT cytoskeletal organization (Fig. 6E-E″,G-G″) compared with control embryos (Fig. 6D-D″,F-F″). These disruptions are particularly striking near the leading edge, as has been observed with other cytoskeletal mutants such as the Rho1 small GTPase (Magie et al., 2002). Similar to embryos, we find that S2R+ cells treated with Syph dsRNA exhibit fewer cellular extensions than their untreated counterparts. In addition, the regular latticework of MTs observed in untreated cells (Fig. 6H,H′) is disrupted in Syph dsRNA-treated cells, with many aggregates of tubulin accumulating within the cell body (Fig. 6I,I′).

DISCUSSION

Dorsal closure is a complex morphogenetic process that is dependent on cell protrusions that are highly dynamic, requiring F-actin filaments and microtubules present in the structures to grow and shrink very rapidly (cf. Rodriguez et al., 2003). Transport of proteins to and within these protrusions and the leading edge is essential for the environmental sensing, cell-cell recognition and adhesion events that take place during DC. Here we present the first characterization of the *Drosophila* myosin XV homolog, Sisyphus, and show that it is required for DC during at least two key steps: for proper epithelial alignment, and for zippering and fusion of the two epithelial sheets. Live imaging of Syph shows that this motor protein accumulates at the leading edge during DC, whereas our mapping and RNAi studies demonstrate interactions with its cargo proteins (Fig. 3), consistent with a role as a transport protein. Our results also suggest a possible role for Syph in the coordination of the actin and MT networks required for the dynamic protrusions during DC.

The MyoX MyTH-FERM myosin has been proposed to play a structural role by facilitating actin polymerization at filopodia tips by pushing the plasma membrane away from the growing actin filament barbed ends to create a space for actin monomer addition

(cf. Sousa and Cheney, 2005). Although Syph is present at filopodium ends and could perform a similar role for actin or MT assembly, unlike MyoX, it is not preferentially found at tips. Instead, Syph moves bi-directionally within LE cells and their protrusions (Fig. 2F-J′; see Movies 1 and 2 in the supplementary material). Reduction of Syph by RNAi disrupts filopodia formation, and this probably contributes to the segment mismatching and zippering/fusion phenotypes observed in *syph*-deficient embryos. *Dictyostelium* cells mutant for the myosin-VII MyTH-FERM protein have also been shown to exhibit loss of filopodia and adhesion defects (Titus, 1999; Tuxworth et al., 2001). How filopodial formation is disturbed in *syph*-deficient embryos remains to be answered, though improper distribution of cargo proteins required for proper filopodial dynamics and integrity of the leading edge is a strong possibility. Another interesting and nonexclusive model is that disruption of the actin-microtubule network caused by Syph knockdown in turn disrupts filopodial formation and/or integrity of the leading edge. Additional studies will be required to differentiate between these two possibilities.

Our mapping data shows that Syph appears to play a key role in transporting structural, adhesive and regulatory molecules within filopodia via its C-terminal FERM domain (Fig. 3). This is consistent with studies in mammals that show that, in addition to the motor domain, the FERM domain of MyoXV is critical for development of stereocilia required for normal hearing and balance (Anderson et al., 2000). One Syph cargo we identified that binds to the FERM domain of Syph is DE-cadherin (Table 1). Cadherin is required at filopodium ends where it forms transient cell-cell contacts, followed by more permanent cell adhesion ones. Here we show that *syph*-deficient embryos are defective in epithelial fusion during DC, presumably due to the failure of cadherin to correctly accumulate at the dorsal-most edge of LE cells to mediate fusion and adhesion. Interestingly, this ‘failure to close’ phenotype is reminiscent of that observed in Rac GTPase mutants proposed to interfere with the contact-inhibition machinery (Woolner et al., 2005). Our results may have clinical relevance, since mutations in the X, VIIA and XV classes of MyTH-FERM unconventional myosins have been shown to cause deafness and aberrant morphology of stereocilia in inner-ear hair cells. Interestingly, in addition to MyoVIIa alleles, mapping of recessive mutations for the most common form of hereditary deaf-blindness in humans, Usher syndrome, has identified alleles of cadherin-23 and protocadherin-15 (Libby and Steel, 2000; Reiners et al., 2006). The MyoVIIa MyTH-FERM myosin has also been shown to interact with cadherin complexes through the vezatin adaptor protein (Kussel-Andermann et al., 2000). Together, these observations suggest that proper distribution and localization of cadherin is essential for normal stereocilia formation or maintenance and may be a conserved task among MyTH-FERM unconventional myosins.

In addition, we mapped the binding site for Syph on DE-cadherin to a C-terminal 40aa fragment of the cad^{ICD} (Fig. 3I). The *Drosophila* genome contains 17 cadherin proteins in addition to DE-cadherin (Hill et al., 2001); we found that three of these show conservation within this C-terminal 40aa motif. Interestingly, this region of DE-cadherin has not been previously assigned a function, but shows conservation with over 15 human cadherins (see Fig. S2D in the supplementary material), and thus may define a novel unconventional myosin-binding domain by which cadherins are tethered and transported.

A remarkable recent finding is the presence of and requirement for MTs in filopodia, as well as in the final stages of zippering during fly DC (Jankovics and Brunner, 2006; Schober et al., 2007). Although unconventional myosins have been generally considered as actin-based motor proteins, members of the MyTH-FERM class were recently shown to bind to and travel along MTs via their MyTH4 domains (Weber et al., 2004). Thus, in addition to trafficking on actin, Syph could traffic on MTs through its two MyTH4 domains. Dynamic MTs have been proposed to work by regulating local concentrations of the cadherin needed to establish and maintain cell-cell contacts (Stehbens et al., 2006), or by delivering actin-organizing proteins to filopodia tips (Basu and Chang, 2007). Thus, Syph could use MTs both as a transport substrate, and be involved in their dynamic assembly/disassembly.

Another appealing possibility is that Syph may play a role in coordinating the two cytoskeletons. Several of the putative cargos we identified for Syph are MT-associated proteins: α-tubulin, Katanin-60, Milt and EB1 are all MT components or binding partners (Table 1). Transport of the MT subunit, α-tubulin, and the MT-severing protein, Katanin-60, suggest a role for Syph in the assembly and disassembly of MTs, whereas the plus end MT-binding protein EB1 suggests a role in stabilization and regulation. A recent study has shown that ectopic expression of another *Drosophila* MT-severing protein, spastin, resulted in delayed epithelial hole closure [taking about 9 hours instead of 3 hours to reaching completion (Jankovics and Brunner, 2006)]. The similar phenotype that we observe in *syph*-deficient embryos suggests that Syph modulates MT cytoskeleton regulation by transporting cargo proteins essential for its regulation.

Our identification of cadherin and several MT-linked proteins as Syph cargos and the mutually exclusive – and perhaps competitive – binding for these cargos on the Syph FERM domain (Fig. 3), leads us to propose that one role of Syph is to coordinate the actin and MT networks during filopodial dynamics through differential cargo transport. Consistent with this possibility, we find that both α-tubulin and actin overexpression rescues the Syph ‘failure to close’ phenotype, and in the case of actin, the delayed closure phenotype as well. These results suggest that the actin network can partially compensate for disruption of the MT one, and that Syph, in addition to serving as a delivery system, may play a role in the regulation of actin and MT cytoskeleton cross-talk during processes such as DC. The finding that the binding sites for putative cargo proteins are mutually exclusive implies that Syph itself must be regulated by proteins that help it ‘choose’ particular proteins to transport. Future studies aimed at uncovering and deciphering the rules governing the choice of cargo and transport substrate for unconventional myosin motors are likely to provide exciting new insight into the coordinate regulation of and cross-talk between the actin and MT cytoskeletons during highly orchestrated morphogenetic events such as DC.

We thank Paul Martin for his interest in the early stages of the project. We also thank Amir Oryan, Phil Soriano, Valera Vasioukhin, and members of the lab for their input during the course of this work and for comments on the manuscript. We are grateful to D. Brunner, C. Delidakis, A. Kaya, H. Oda, J. Tenlen, R. Tsien, the DGRC, and the Bloomington/Kyoto Stock Centers for antibodies, flies and other reagents used in this study. This work was supported by NIH grant GM066847 to S.M.P.

Supplementary material

Supplementary material for this article is available at http://dev.biologists.org/cgi/content/full/135/1/53/DC1

References

Anderson, D. W., Probst, F. J., Belyantseva, I. A., Fridell, R. A., Beyer, L., Martin, D. M., Wu, D., Kachar, B., Friedman, T. B., Raphael, Y. et al. (2000). The motor and tail regions of myosin XV are critical for normal structure and function of auditory and vestibular hair cells. *Hum. Mol. Genet.* **9**, 1729-1738.

Basu, R. and Chang, F. (2007). Shaping the actin cytoskeleton using microtubule tips. *Curr. Opin. Cell Biol.* **19**, 88-94.

Berg, J. S. and Cheney, R. E. (2002). Myosin-X is an unconventional myosin that undergoes intrafilopodial motility. *Nat. Cell Biol.* **4**, 246-250.
Berg, J. S., Powell, B. C. and Cheney, R. E. (2001). A millennial myosin census. *Mol. Biol. Cell* **12**, 780-794.
Bohil, A. B., Robertson, B. W. and Cheney, R. E. (2006). Myosin-X is a molecular motor that functions in filopodia formation. *Proc. Natl. Acad. Sci. USA* **103**, 12411-12416.
Brand, A. H. and Perrimon, N. (1993). Targeted gene expression as a means of altering cell fates and generating dominant phenotypes. *Development* **118**, 401-415.
Faix, J. and Rottner, K. (2006). The making of filopodia. *Curr. Opin. Cell Biol.* **18**, 18-25.
Foth, B. J., Goedecke, M. C. and Soldati, D. (2006). New insights into myosin evolution and classification. *Proc. Natl. Acad. Sci. USA* **103**, 3681-3686.
Gibson, F., Walsh, J., Mburu, P., Varela, A., Brown, K. A., Antonio, M., Beisel, K. W., Steel, K. P. and Brown, S. D. (1995). A type VII myosin encoded by the mouse deafness gene shaker-1. *Nature* **374**, 62-64.
Hill, E., Broadbent, I. D., Chothia, C. and Pettitt, J. (2001). Cadherin superfamily proteins in *Caenorhabditis elegans* and *Drosophila melanogaster*. *J. Mol. Biol.* **305**, 1011-1024.
Jacinto, A., Woolner, S. and Martin, P. (2002). Dynamic analysis of dorsal closure in *Drosophila*: from genetics to cell biology. *Dev. Cell* **3**, 9-19.
Jankovics, F. and Brunner, D. (2006). Transiently reorganized microtubules are essential for zippering during dorsal closure in *Drosophila melanogaster*. *Dev. Cell* **11**, 375-385.
Kang, B. S., Cooper, D. R., Devedjiev, Y., Derewenda, U. and Derewenda, Z. S. (2002). The structure of the FERM domain of merlin, the neurofibromatosis type 2 gene product. *Acta Crystallogr. D Biol. Crystallogr.* **58**, 381-391.
Kiehart, D. P., Franke, J. D., Chee, M. K., Montague, R. A., Chen, T. L., Roote, J. and Ashburner, M. (2004). Drosophila crinkled, mutations of which disrupt morphogenesis and cause lethality, encodes fly myosin VIIA. *Genetics* **168**, 1337-1352.
Kussel-Andermann, P., El-Amraoui, A., Safieddine, S., Nouaille, S., Perfettini, I., Lecuit, M., Cossart, P., Wolfrum, U. and Petit, C. (2000). Vezatin, a novel transmembrane protein, bridges myosin VIIA to the cadherin-catenins complex. *EMBO J.* **19**, 6020-6029.
Liang, Y., Wang, A., Belyantseva, I. A., Anderson, D. W., Probst, F. J., Barber, T. D., Miller, W., Touchman, J. W., Jin, L., Sullivan, S. L. et al. (1999). Characterization of the human and mouse unconventional myosin XV genes responsible for hereditary deafness DFNB3 and shaker 2. *Genomics* **61**, 243-258.
Libby, R. T. and Steel, K. P. (2000). The roles of unconventional myosins in hearing and deafness. *Essays Biochem.* **35**, 159-174.
Magie, C. R. and Parkhurst, S. M. (2005). Rho1 regulates signaling events required for proper *Drosophila* embryonic development. *Dev. Biol.* **278**, 144-154.
Magie, C. R., Pinto-Santini, D. and Parkhurst, S. M. (2002). Rho1 interacts with p120ctn and α-catenin, and regulates cadherin-based adherens junction formation during *Drosophila* development. *Development* **129**, 3771-3782.
Mermall, V., Post, P. L. and Mooseker, M. S. (1998). Unconventional myosins in cell movement, membrane traffic, and signal transduction. *Science* **279**, 527-533.
Oda, H. and Tsukita, S. (1999). Nonchordate classic cadherins have a structurally and functionally unique domain that is absent from chordate classic cadherins. *Dev. Biol.* **216**, 406-422.
Oliver, T. N., Berg, J. S. and Cheney, R. E. (1999). Tails of unconventional myosins. *Cell. Mol. Life Sci.* **56**, 243-257.
Poortinga, G., Watanabe, M. and Parkhurst, S. M. (1998). *Drosophila* CtBP: a Hairy-interacting protein required for embryonic segmentation and Hairy-mediated transcriptional repression. *EMBO J.* **17**, 2067-2078.
Raich, W. B., Agbunag, C. and Hardin, J. (1999). Rapid epithelial-sheet sealing in the *Caenorhabditis elegans* embryo requires cadherin-dependent filopodial priming. *Curr. Biol.* **9**, 1139-1146.
Reiners, J., Kerstin, N., Jurgens, K., Marker, T. and Wolfrum, U. (2006). Molecular basis of human Usher syndrome: deciphering the meshes of the Usher protein network provides insights into the pathomechanisms of the Usher disease. *Exp. Eye Res.* **83**, 97-119.
Ridley, A. J., Schwartz, M. A., Burridge, K., Firtel, R., Ginsberg, M. H., Borisy, G., Parsons, T. H. and Horwitz, A. R. (2003). Cell migration: integrating signals from front to back. *Science* **302**, 1704-1709.
Rodriguez, O. C., Schaefer, A. W., Mandato, C. A., Forscher, P., Bement, W. M. and Waterman-Storer, C. M. (2003). Conserved microtubule-actin interactions in cell movement and morphogenesis. *Nat. Cell Biol.* **5**, 599-609.
Rosales-Nieves, A. E., Johndrow, J. E., Keller, L. C., Magie, C. R., Pinto-Santini, D. and Parkhurst, S. M. (2006). Coordination of microtubule and microfilament dynamics by *Drosophila* Rho1, Spire, and Cappuccino. *Nat. Cell Biol.* **8**, 367-376.
Schober, J. M., Komarova, Y. A., Chaga, O. Y., Akhmanova, A. and Borisy, G. G. (2007). Microtubule-targeting-dependent reorganization of filopodia. *J. Cell Sci.* **120**, 1235-1244.
Shaner, N. C., Campbell, R. E., Steinbach, P. A., Giepmans, B. N., Palmer, A. E. and Tsien, R. Y. (2004). Improved monomeric red, orange and yellow fluorescent proteins derived from Discosoma sp. red fluorescent protein. *Nat. Biotechnol.* **22**, 1567-1572.
Sheetz, M. P. (1999). Motor and cargo interactions. *Eur. J. Biochem.* **262**, 19-25.
Sousa, A. D. and Cheney, R. E. (2005). Myosin-X: a molecular motor at the cell's fingertips. *Trends Cell Biol.* **15**, 533-539.
Spradling, A. C. (1986). P element-mediated transformation. In *Drosophila, A Practical Approach* (ed. D. B. Roberts), pp. 175-197. Oxford: IRL Press.
Stehbens, S. J., Paterson, A. D., Crampton, M. S., Shewan, A. M., Ferguson, C., Akhmanova, A., Parton, R. G. and Yap, A. S. (2006). Dynamic microtubules regulate the local concentration of E-cadherin at cell-cell contacts. *J. Cell Sci.* **119**, 1801-1811.
Titus, M. A. (1999). A class VII unconventional myosin is required for phagocytosis. *Curr. Biol.* **9**, 1297-1303.
Todi, S. V., Franke, J. D., Kiehart, D. P. and Eberl, D. F. (2005). Myosin VIIA defects, which underlie the Usher 1B syndrome in humans, lead to deafness in *Drosophila*. *Curr. Biol.* **15**, 862-868.
Tuxworth, R. I., Weber, I., Wessels, D., Addicks, G. C., Soll, D. R., Gerisch, G. and Titus, M. A. (2001). A role for myosin VII in dynamic cell adhesion. *Curr. Biol.* **11**, 318-329.
Tzolovsky, G., Millo, H., Pathirana, S., Wood, T. and Bownes, M. (2002). Identification and phylogenetic analysis of Drosophila melanogaster myosins. *Mol. Biol. Evol.* **19**, 1041-1052.
Vasioukhin, V. and Fuchs, E. (2001). Actin dynamics and cell-cell adhesion in epithelia. *Curr. Opin. Cell Biol.* **13**, 76-84.
Verkhusha, V. V., Tsukita, S. and Oda, H. (1999). Actin dynamics in lamellipodia of migrating border cells in the Drosophila ovary revealed by a GFP-actin fusion protein. *FEBS Lett.* **445**, 395-401.
Weber, K. L., Sokac, A. M., Berg, J. S., Cheney, R. E. and Bement, W. M. (2004). A microtubule-binding myosin required for nuclear anchoring and spindle assembly. *Nature* **431**, 325-329.
Weil, D., Blanchard, S., Kaplan, J., Guilford, P., Gibson, F., Walsh, J., Mburu, P., Varela, A., Levilliers, J., Weston, M. D. et al. (1995). Defective myosin VIIA gene responsible for Usher syndrome type 1B. *Nature* **374**, 60-61.
Woolner. S., Jacinto, A. and Martin, P. (2005). The small GTPase Rac plays multiple roles in epithelial sheet fusion–dynamic studies of Drosophila dorsal closure. *Dev. Biol.* **282**, 163-173.
Zhang, H., Berg, J. S., Li, Z., Wang, Y., Lang, P., Sousa, A. D., Bhaskar, A., Cheney, R. E. and Stromblad, S. (2004). Myosin-X provides a motor-based link between integrins and the cytoskeleton. *Nat. Cell Biol.* **6**, 523-531.